


A Compact Low-Power Current-to-Digital Readout Circuit for Amperometric Electrochemical Sensors

Heyu Yin , Ehsan Ashoori, *Student Member, IEEE*, Xiaoyi Mu, *Member, IEEE*, and Andrew J. Mason, *Senior Member, IEEE*

Abstract—This paper introduces a novel compact low-power amperometric instrumentation design with current-to-digital output for electrochemical sensors. By incorporating the double layer capacitance of an electrochemical sensor's impedance model, our new design can maintain performance while dramatically reducing circuit complexity and size. Electrochemical experiments with potassium ferricyanide show that the circuit output is in a good agreement with results obtained using commercial amperometric instrumentation. A high level of linearity ($R^2 = 0.991$) between the circuit output and the concentration of potassium ferricyanide was also demonstrated. Furthermore, we show that a CMOS implementation of the presented architecture could save 25.3% of the area and 47.6% of power compared to a traditional amperometric instrumentation structure. Thus, this new circuit structure is ideally suited for portable/wireless electrochemical sensing applications.

Index Terms—Amperometric instrumentation, compact, current-to-digital readout, electrochemical sensor, low power.

I. INTRODUCTION

ELECTROCHEMICAL sensors are widely used for environmental monitoring such as gaseous pollutants [1], and medical/healthcare diagnosis such as detection of antigen-antibody binding events, hybridized DNA, neuronal tissue, bacteria, glucose, and enzymes reaction [2]. The most prevalent electrochemical sensor mode is the amperometric mode, in which the sensor reaction current is proportional to the analyte concentration. Recently, there is a trend in developing sensor microsystem for wireless, portable, and implantable monitoring applications. These applications bring extreme requirements for instrumentation circuits in terms of power, area, and cost, especially in applications that demand a large number of sensors [3].

Manuscript received November 19, 2018; revised May 2, 2019; accepted May 23, 2019. Date of publication June 10, 2019; date of current version April 7, 2020. This work was supported in part by the National Institutes of Health under Grant NIH_R01ES022302 and in part by the National Institute for Occupational Safety and Health (NIOSH) under Grant R01OH009644. The Associate Editor coordinating the review process was Fabricio Baptista. (Corresponding author: Heyu Yin.)

H. Yin, E. Ashoori, and A. J. Mason are with the Department of Electrical and Computer Engineering, Michigan State University, East Lansing, MI 48824 USA (e-mail: yinheyu@msu.edu).

X. Mu is with Apple Inc., Cupertino, CA 95014 USA.

Color versions of one or more of the figures in this article are available online at <http://ieeexplore.ieee.org>.

Digital Object Identifier 10.1109/TIM.2019.2922053

Amperometric instrumentation consists of two parts: a potentiostat and a current readout circuit. The potentiostat provides the current required for the reaction while maintaining the electrode/electrolyte interface at the correct potential. The current readout circuit conditions the electrochemical measurement and digitizes the reaction current. It is common to use bulky instrumentation to collect the amperometric readout. Many of the electrochemical instruments reported utilize commercial instrumentation and do not focus on the challenges of miniaturization for portable applications [4], [5]. However, the bulky instrumentation is expensive and not good for system miniaturization. Existing research has focused on optimizing individual parts (either potentiostat or readout circuit) for given power/size/resolution requirements [6]–[12], which help to push forward the circuit design for portable/wireless electrochemical sensing applications. However, no research has considered topology optimization from the perspective of the complete sensor-circuit system level. A great deal of recent research has focused on CMOS amperometric circuit designs for specific applications [13]–[21]. However, for many low volume and research applications, the economics of CMOS is not beneficial, and a simple amperometric circuit that is easy to build and can perform well without CMOS fabrication would be of great value.

This paper introduces a novel compact and low-power amperometric instrumentation circuit topology that utilizes the inherent nature of electrochemical sensor interfaces to enable system-level optimization. The new amperometric circuit provides complete current-to-digital readout with reduced component count compared to traditional amperometric instrumentation. Specifically, our new topology saves two operational amplifiers (opamp) and one integrator capacitor, and thus significantly lowering circuit power and area compared to a traditional design. Therefore, the new electrochemical instrumentation circuit is well-suited for portable, wireless, and implantable sensory microsystem applications. This paper makes major reuse of the content in Xiaoyi's [22] thesis with permission.

Section II introduces the electrochemical sensor model and the traditional amperometric instrumentation circuit. Section III details the new compact amperometric instrumentation design concept. Section IV presents performance comparisons to traditional instrumentation circuits and evaluates the

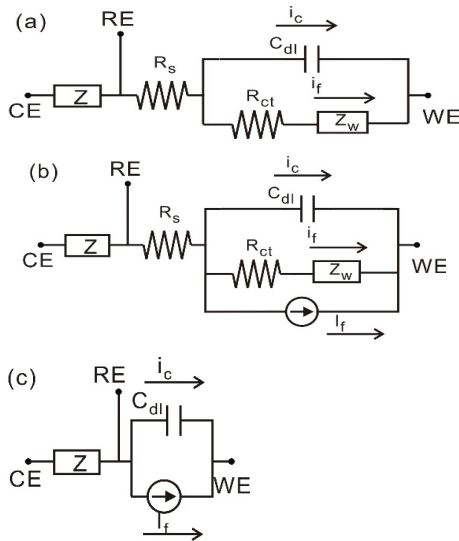


Fig. 1. Equivalent circuit model of electrochemical sensor cell. (a) Randles model. (b) Complete model considering both ac and dc stimulus. (c) Simplified model for circuit analysis.

errors caused by model simplification. Circuit implementation and test results are shown in Section IV, and a conclusion is presented in Section V.

II. ELECTROCHEMICAL SENSOR MODEL AND TRADITIONAL AMPEROMETRIC INSTRUMENTATION CIRCUITS

A. Electrochemical Sensor and Its Equivalent Circuit Model

Electrochemical sensors in amperometric mode work under the following sensing principle: the reaction current is proportional to the analyte concentration when reacted electrode/electrolyte interface is biased at a constant voltage. To accurately control the reaction taking place at the interface, three-electrode cell configuration has been applied to amperometric electrochemical sensors. In such a three-electrode cell, the reaction takes place at the interface between the working electrodes (WE) and electrolyte. A constant potential is maintained between the reference electrode (RE) and the WE. The third electrode, the counter electrode (CE), provides a current path to the WE.

To analyze the electrochemical sensor's electrical response, equivalent circuit models have been proposed in electrochemical impedance spectroscopy (EIS) theory. Randles circuit model [23], as shown in Fig. 1(a), is a classic equivalent circuit model widely used to describe a three-electrode sensor. The impedance between the RE and the WE consists of an uncompensated solution resistor R_s (relatively small), in series with the parallel combination of the double-layer capacitor C_{dl} at the WE interface (charging current i_c follows through this path), and an impedance of a faradaic reaction caused by ac stimulus (ac faradaic current i_f follows through this path). The faradaic reaction consists of a charge transfer resistor R_{ct} and Warburg element Z_w which can be calculated as

$$Z_w = \frac{A_w}{\sqrt{j\omega}} \quad (1)$$

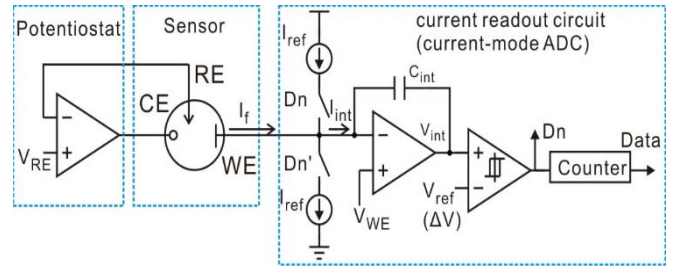


Fig. 2. Schematic of a model amperometric instrumentation circuit including potentiostat and current-mode $\Sigma \Delta$ ADC.

where A_w is the Warburg coefficient and ω is the angular frequency. Since our only interest is in the WE interface, the impedance between the CE and the RE is denominated as simple impedance Z . Notice that this model only represents the sensor's response to a small ac stimulus. To represent both ac and dc response, a complete equivalent circuit model is shown in Fig. 1(b) [23], [24]. A current source is added to represent dc faradaic current I_f . Here, I_f is the constant reaction current proportional to the analyte concentration in amperometric electrochemical sensors, which is the main interest in sensor current measurements. In general, $i_f \ll I_f$, and R_s is relatively small. They can be considered as second-order effects in sensors response. For analysis simplicity, R_s and $i_{f,ac}$ are omitted during following instrumentations derivation and are rediscussed in Section III. The simplified model is shown in Fig. 1(c).

B. Traditional Amperometric Instrumentation

As introduced in Section I, the amperometric instrumentation circuit consists of two parts: a potentiostat and a current readout circuit. The potentiostat provides current from the CE to the WE while maintaining the voltage between the RE and the WE. A typical potentiostat can be implemented by a single opamp with appropriate connections [9], [25], [26]: the positive input node is connected with bias for the RE (V_{RE}), the negative input node is connected to the RE, and the output is connected with the CE to provide the current path. The current readout circuit collects I_f either at the WE or the CE, then conditions and digitizes it. Two topologies have been used to implement the current readout circuit: a current-to-voltage converter followed by a voltage-mode analog-to-digital converter (ADC) [27] and a single current-mode ADC [11], [28]. Given the requirement of sensor applications for low power and low complexity, a model amperometric instrumentation circuit, as shown in Fig. 2, utilizes the single opamp for potentiostat design and the current-mode ADC for current readout design. In the current-mode ADC, two reference current sources I_{ref} of opposite direction are alternately connected with the integrator through switches, which are controlled by the digital output of the hysteresis comparator Dn . Thus, the input current of the integrator I_{int} is given by

$$I_{int} = I_f - (-1)^{Dn} \cdot I_{ref}. \quad (2)$$

In Fig. 3, waveforms illustrate that the integrator capacitor is charged/discharged according to the direction of I_{int} .

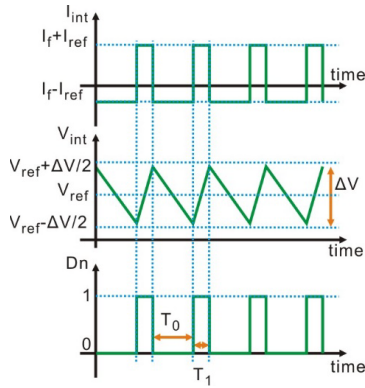


Fig. 3. Waveforms of the current on the integrator input I_{int} , the voltage on the integrator output V_{int} , and the digital output of the comparator Dn .

Consequently, the output of the integrator V_{int} rises/falls corresponding to I_{int} direction. While V_{int} reaches the hysteresis comparator upper/lower bound ($V_{ref} +/\Delta V/2$) (where ΔV is the hysteresis window width and V_{ref} is the reference voltage), Dn flips, changing I_{int} according to (2). The square waveform at the output of the hysteresis comparator is then digitized by a counter with the reference clock at a much higher frequency. The time interval T_1 of the digital “high” for Dn is given by

$$T_0 = \frac{C_{int} \cdot \Delta V}{I_{ref} + I_f} \quad (3)$$

and the time interval T_0 of the digital “low” for Dn is

$$T_0 = \frac{C_{int} \cdot \Delta V}{I_{ref} - I_f}. \quad (4)$$

From (3) and (4), I_f can be expressed as a function of I_{ref} , T_1 , and T_0 by

$$I_f = \frac{T_0 - T_1}{T_0 + T_1} I_{ref}. \quad (5)$$

If the duty cycle α of Dn is defined as

$$\alpha = \frac{T_1}{T_1 + T_0} \quad (6)$$

later by combining (5) and (6), I_f can be expressed as a function of α and I_{ref} is given by

$$I_f = (1 - 2\alpha) \cdot I_{ref}. \quad (7)$$

Therefore, given a known I_{ref} , I_f is obtained by measuring the duty cycle of Dn . Notice that I_f is independent of both the integrator capacitor C_{int} and the hysteresis comparator parameters (ΔV and V_{ref}).

III. COMPACT AMPEROMETRIC INSTRUMENTATION DESIGN

In the model amperometric instrumentation circuit in Fig. 2, replacing the sensor symbol with the simplified electrochemical sensor equivalent circuit model in Fig. 1(c) produces the fully electrical schematic of an electrochemical sensor system shown in Fig. 4. Notice that the sensor operates at the steady state when no current flows through C_{dl} and only I_f is collected in the readout circuit. From a system point of view,

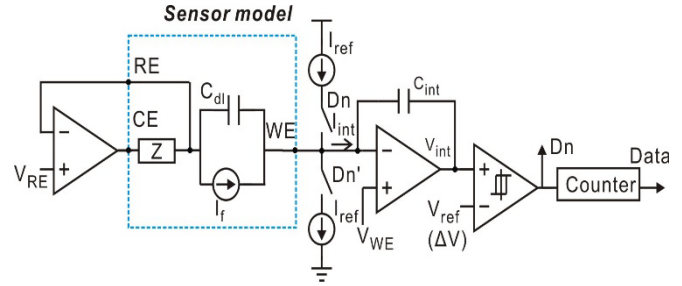


Fig. 4. Schematic of the electrochemical sensor system consisting of a model amperometric instrumentation circuit and the simplified electrochemical sensor equivalent circuit model.

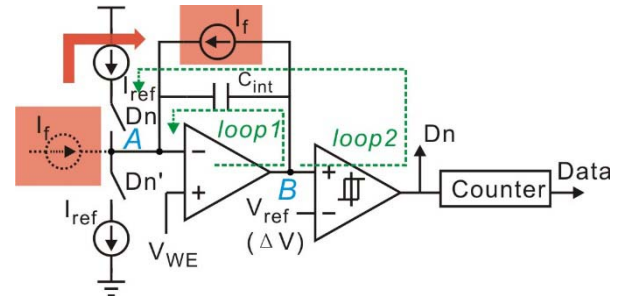


Fig. 5. Derivation of the instrumentation topology. The input current source is folded into parallel connection with the integrator capacitor.

the sensor system contains two capacitors: C_{dl} and C_{int} . C_{int} is part of the readout circuit and used for charging/discharging; C_{dl} is the inherent interface capacitor. Since capacitors occupy a large area in integrated circuits, if C_{dl} could be utilized to play the role of C_{int} , then C_{int} could be eliminated from the circuit to save area. Modifying the traditional structure to incorporate C_{dl} into the circuit and eliminate C_{int} , we develop a compact amperometric instrumentation topology.

As shown in Fig. 5, a current source I_f can be used to represent the electrochemical sensor equivalent model. Given that node B is a low-impedance node, folding the current source to the output of the integrator is equivalent to the typical topology of the current readout circuit. Notice that the parallel connection of I_f and C_{int} is the same as the equivalent circuit between RE and WE in Fig. 1(c). Since the value C_{int} is arbitrary, I_f still can be calculated from (7) when C_{int} is replaced with C_{dl} .

To satisfy sensor’s bias condition, a potentiostat function is incorporated into the current-mode ADC by the following modification steps. First, by flipping the direction of I_f , and substituting V_{ref} and V_{WE} with V_{WE} and V_{RE} , the voltage between the RE and the WE can be held by feedback loops of the integrator (loop1) and of the ADC (loop2). Although WE potential is not strictly held constant due to a nonzero value of ΔV in the loop2, the perturbation on WE does not affect the sensor’s steady state as long as ΔV is set small enough (less than 10 mV) [29]. In addition, because the current can only flow from the CE to the WE, node A should be connected to CE rather than RE.

Following the modification described above, a modified amperometric instrumentation circuit with the sensor model can be shown in Fig. 6. However, the direction of the current

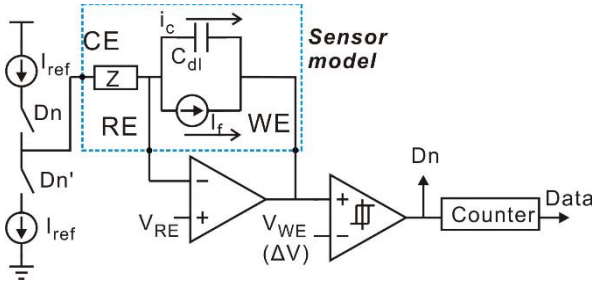


Fig. 6. Schematic of the modified amperometric instrumentation circuit with the sensor equivalent circuit model.

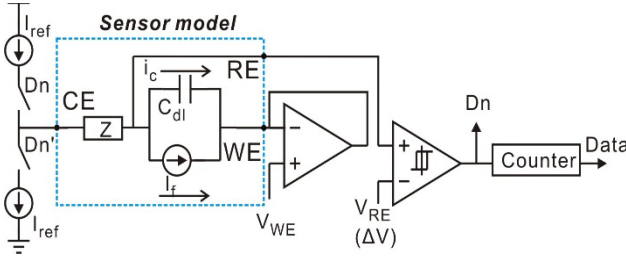


Fig. 7. Schematic of the simplified compact amperometric instrumentation circuit with the electrochemical sensor equivalent circuit model.

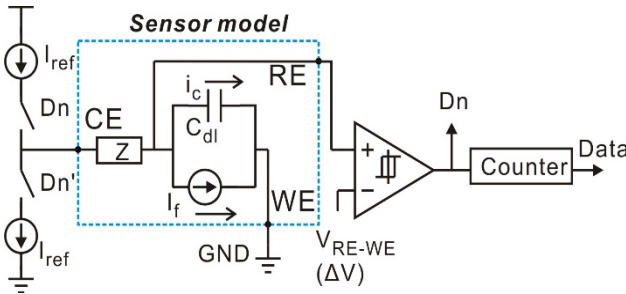


Fig. 8. Schematic of CCDAI with the electrochemical sensor equivalent circuit model.

source I_f is opposite from the direction of I_f in Fig. 5, I_f in Fig. 6 should be written as

$$I_f = (2\alpha - 1) \cdot I_{\text{ref}}. \quad (8)$$

This topology successfully realizes the functions of both current-mode ADC and potentiostat. Compared to a traditional topology in Fig. 2, it utilizes C_{dl} for the integrator and eliminates one opamp required by the potentiostat and C_{int} required by the integrator. Note that voltages at RE and WE in Fig. 6 are both held by the feedback loops and no constraints are required for V_{RE} and V_{WE} from circuit perspective. Therefore, nodes RE and WE are interchangeable. By swapping WE with RE, the simplified structure shown in Fig. 7 can be achieved. Note the connection of WE to a unit-gain buffer and this buffer can be discarded for further simplification. By connecting the WE to the ground and replacing V_{RE} with $V_{\text{RE-WE}}$, the resulting schematic in Fig. 8 shows a new compact current-to-digital amperometric instrumentation (CCDAI) topology. Here, it has been assumed that the sensor bias requires $V_{\text{RE}} > V_{\text{WE}}$ and, thus, $V_{\text{RE-WE}} > 0$. If the sensor bias requires $V_{\text{RE}} < V_{\text{WE}}$, the WE could alternatively be connected to the power supply.

Following the derivation from the schematic in Fig. 4 to the one in Fig. 8, the CCDAI topology was designed functionally equivalent to the traditional amperometric instrumentation when the parameters of the hysteresis comparator in the CCDAI meet the following constraints: V_{ref} is set to $V_{\text{RE-WE}}$, and ΔV is set to 10 mV.

IV. PERFORMANCE ANALYSIS

Although the function of the CCDAI is equivalent to the traditional amperometric instrumentation, structure differences and additional constraints will cause performance differences. In addition, as mentioned in Section I, the equivalent circuit used to derive the circuit topology was the simplified model in Fig. 1(c). The sensors' second-order effects should be fully considered in terms of performance. This section evaluates the performance of the CCDAI in two aspects: performance difference from the traditional amperometric instrumentation and performance affected by second-order elements in the equivalent circuit model.

A. Performance Relative to Traditional Amperometric Instrumentation

Compared to the traditional potentiostat that drives the electrochemical cell from an opamp output, the CCDAI drives the electrochemical cell by a constant current source with much a lower current value. Therefore, it would take a longer time to stabilize the electrochemical cell potential. Nevertheless, differences in the potential stabilization time would not affect the steady-state operation of the electrochemical cell.

Compared to a traditional current mode ADC, the main differences of the CCDAI include: 1) the integrator capacitor C_{int} is replaced by the sensor's double layer capacitor C_{dl} and 2) the hysteresis comparator voltage window is limited to 10 mV. These two differences could affect the resolution of the calculated I_f . From (7), I_f is obtained by calculating measured α with a known I_{ref} value. From (6), the resolution of α is determined by how short T_0 and T_1 are given a fixed counter reference clock frequency. From (3) and (4), T_0 and T_1 are proportional to C_{dl} and ΔV . Therefore, C_{dl} and ΔV do affect the resolution of I_f . Assuming $|I_f| < I_{\text{max}}$, the given max time interval width is expressed by

$$T_{\text{max}} = \frac{C_{\text{dl}} \cdot \Delta V}{I_{\text{ref}} - I_{\text{max}}}. \quad (9)$$

For a fixed counter reference clock frequency f_0 , the maximum relative quantization error [28] is given by

$$|\delta_q|_{\text{max}} = \frac{1}{f_0 \cdot T_{\text{max}}} = \frac{I_{\text{ref}} - I_{\text{max}}}{f_0 \cdot C_{\text{dl}} \cdot \Delta V}. \quad (10)$$

The ADC's effective resolution (in bits) N is determined by

$$N = -\log_2 |\delta_q|_{\text{max}} = \log_2(f_0 \cdot C_{\text{dl}} \cdot \Delta V) - \log_2(I_{\text{ref}} - I_{\text{max}}). \quad (11)$$

Therefore, larger ΔV and C_{dl} would improve the effective resolution N . In the traditional current-mode ADC, ΔV can be up to the power supply voltage, V_{dd} , which can be 5 V in a portable device. In the CCDAI, ΔV is restricted to a maximum

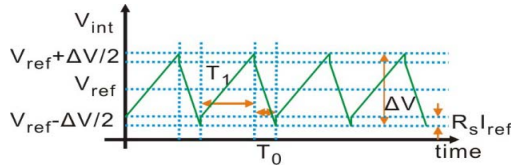


Fig. 9. V_{int} waveform illustration when considering R_s in the equivalent circuit model.

of 10 mV. ΔV in the CCDAI is 500 times smaller than in the traditional current-mode ADC, resulting in 9 bits of effective resolution loss for the CCDAI. However, in the meantime, electrochemical double layer capacitor C_{dl} has much larger capacitance density than a capacitor that can be fabricated by CMOS process in a single IC chip. For instance, a double layer formed on 1 mm² electrode can generate μF level capacitance; while a capacitor in a single IC chip is up to tens of pF. The 10000 times larger capacitance in the CCDAI would result in 13 bits of effective resolution improvement for the CCDAI. Therefore, the total effect of C_{dl} and ΔV provides an improvement of around 4 bits of the effective resolution. As a tradeoff, the sampling rate drops as the effective resolution increases. Fortunately, electrochemical systems typically have a slow response and do not need a fast sampling rate.

B. Second-Order Effects of the Sensor Equivalent Circuit Model

The derivation in Section III was based on a simplified model in Fig. 1(c). Given a complete model in Fig. 1(b), an evaluation is needed to determine whether the solution resistor R_s and ac Faradaic components in the complete equivalent circuit model would introduce significant errors.

If we first consider adding R_s to the circuit, the corresponding waveform of V_{int} is shown in Fig. 9. Although the abrupt jump in V_{int} caused by R_s can be observed, this does not change T_1 and T_0 . Thus, (8) is still valid. However, the abrupt jump decreases the effective charging/discharging window from ΔV to $\Delta V - I_{ref} \cdot R_s$. In a standard electrochemical cell configuration, the RE is placed close to the WE and a typical experimental value of R_s is on the order of 10–10² Ω . With μA level of I_{ref} , this only gives 10–100- μV error, which is less than 1% of 10 mV. Therefore, R_s has a negligible impact on the resolution.

Next, ac Faradaic components were evaluated. The ac Faradaic components are in parallel with the double layer capacitor C_{dl} and the dc Faradaic current source I_f . Since both the Warburg element and C_{dl} block dc current, only ac current i_f can pass through those ac Faradaic components. The sensor current I_{sens} is the sum of the dc current I_f and the ac current $i_c + i_f$. Observe that the sensor current I_{sens} should be equal to the current provided by the current source at any time

$$I_{sens}(t) = I_c + I_{f,ac} + I_{f,dc} = \begin{cases} I_{ref} & \text{during } T_1 \\ -I_{ref} & \text{during } T_0 \end{cases} \quad (12)$$

where T_1 is the time interval when $Dn = 1$ in the CCDAI, T_0 is the time interval when $Dn = 0$ in the CCDAI. Here T_1

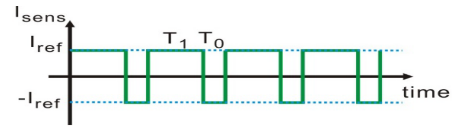


Fig. 10. Illustration of I_{sens} in the time domain.

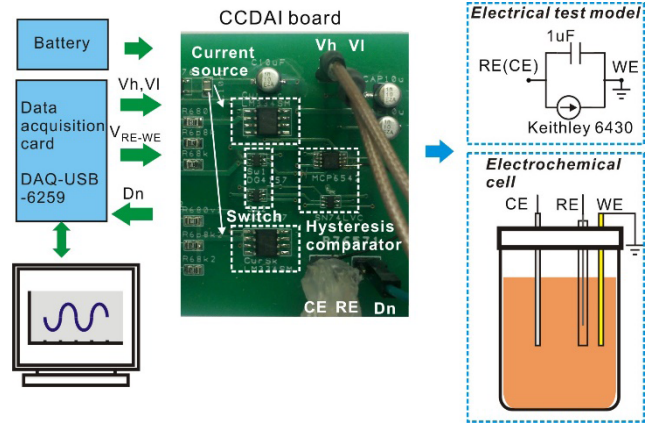


Fig. 11. Test setup for electrical and chemical experiment.

and T_0 do not follow (3) and (4). The waveform of I_{sens} is shown in Fig. 10. Given the waveform in the time domain, I_{sens} can also be expressed by Fourier series as

$$I_{sens} = \left[(2\alpha - 1) + 4 \sum_{k=1}^{\infty} \frac{\sin(k\alpha\pi)}{k\pi} \cos(k \cdot 2\pi f_c \cdot t) \right] I_{ref} \quad (13)$$

where $f_c = 1/(T_1 + T_0)$. The first term in (13) represents the dc part of I_{sens} , and the second term represents the ac part. Since the ac components (C_{dl} and Warburg elements) block dc currents, and dc current source blocks ac currents, I_f is equal to the dc part of I_{sens} . Thus, I_f is

$$I_{f,dc} = (2\alpha - 1) \cdot I_{ref}. \quad (14)$$

As (14) is identical to (7), one can conclude that the readout value of the CCDAI is the same as the result obtained in Section III, even when considering the complete electrochemical sensor equivalent circuit model.

V. RESULTS

A. CCDAI Implementation

To verify the functionality and performance of the CCDAI, the test setup shown in Fig. 11 was built. The CCDAI was implemented on a printed circuit board with the following commercial IC chips: high-precision current source [LM334SM (TI)], high-speed switches [DG4157 (Vishay), turn on/off time—22/8 ns], push-pull output comparator (MCP6542), and the buffer gate (SN74LVC)]. The circuit power supply was set to 5 V and current bias I_{ref} was set to 1 μA , which are suitable values for a portable sensor application. To implement a hysteresis comparator with upper and lower bounds that can be adjusted independently during testing, the circuit shown in Fig. 12 was implemented using

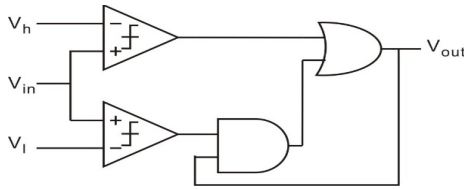


Fig. 12. Hysteresis comparator realization with adjustable upper/lower bound.

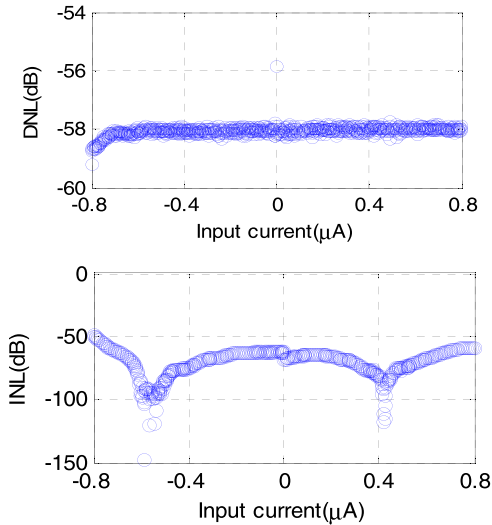


Fig. 13. DNL and INL of the CCDAI. Both DNL and INL in the current range are better than -49 dB, implying an 8 bit of effective resolution.

two comparators, an AND gate, and an OR gate. A USB-6259 data acquisition card (National Instrumentations Inc.) was used to set the voltage on the reference electrode, V_{RE-WE} , and the comparator's upper/lower bound voltages, V_h and V_l . It was also used to measure the time intervals T_1 and T_0 of comparator output Dn using an internal 10 MHz clock. A LabView user interface was built for communication between a PC and the data acquisition card. The current I_f was calculated using (8) with the measured T_1 and T_0 values.

B. Experimental Results

To evaluate the ADC performance of the CCDAI, an electrical test model was connected with the CCDAI board. To implement the simplified model in Fig. 1(c), the electrical test model consisted of a $1 \mu\text{F}$ capacitor and a Keithley 6430 Source Meter connected in parallel. CE and RE were shorted in the test. The current readout accuracy of the CCDAI was tested by sweeping I_f from -800 to 800 nA with 2 nA step. Differential nonlinearity (DNL) and integral nonlinearity (INL) of the readout current are shown in Fig. 13. The worst DNL equals to -56 dB and the worst INL equals to -49 dB, meaning that CCDAI achieves a resolution of better than 6 nA, equivalent to 8 bits over the tested range. To increase the resolution of the CCDAI, tradeoffs with other performance metrics could be considered. For example, as shown in (11) the main factors to determine resolution are ΔV , C_{dl} , and f_0 . In theory, the resolution is enhanced by increasing ΔV . However, as described in Section III,

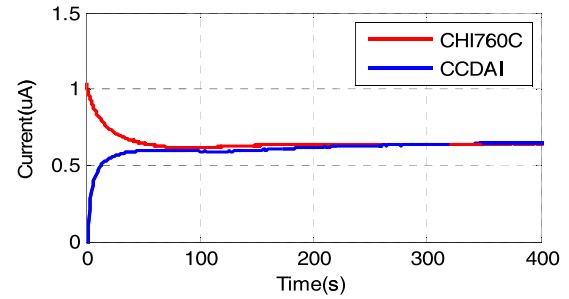


Fig. 14. Faradaic current generated by 6 mM of potassium ferricyanide as function of time when $V_{WE-RE} = 190$ mV. Red line represents data recorded by CHI760C and blue line represents data recorded by CCDAI.

ΔV has to be set to less than 10 mV to avoid inaccuracy in RE-WE voltage and degradation of the electrochemical result. C_{dl} is an inherent parameter of the electrochemical cell and is already much higher than the capacitors implemented on-chip in conventional CMOS designs. The resolution could be enhanced by increasing f_0 at the expense of higher power consumption. Considering this tradeoff, in our design, we set the f_0 as 100 kHz. It is a remarkable fact that increasing f_0 for better resolution not only increases the power consumption of the counter but also increases the size of the counter to support a greater number of bits. Therefore, by considering a fixed counter clock frequency of $f_0 = 100$ kHz, the 8-bit resolution has been implemented which enables us to reach 6 -nA resolution. This resolution meets the requirements for many electrochemical sensor applications [30].

To verify the electrochemical functionality of the CCDAI board, an electrochemical test was performed using an electrochemical cell with potassium ferricyanide as the analyte. The electrolyte consists of 0.1 -M potassium chloride as a buffer solution and potassium ferricyanide with varying concentrations (from 0 to 6 mM). Ag/AgCl (CH Instrumentations Inc.) was used as standard RE. Pt wire (CH Instrumentations Inc.) was used as the CE. Au plate with 1 mm² area (CH Instrumentations Inc.) was used as the WE. V_{WE-RE} was set to 190 mV.

The faradaic current generated by potassium ferricyanide redox reaction was recorded by the CCDAI as a function of time. The commercial electrochemical instrumentation CHI760C was used as a reference to record current data at the same condition setup. As an example, data for a 6 mM concentration is shown in Fig. 14 that both the currents recorded by CCDAI and CHI760C converged to the same level with negligible differences after the chemical system reached the steady state. The transit pattern differences are caused by the different stimulus provided by the two instrumentations. CHI760C applies large current to set the initial V_{WE-RE} to the desired voltage in the very short time; while CCDAI applies a constant current to raise V_{WE-RE} to the desired voltage in a gentle way. In addition, the initial current recorded by CHI760C includes charging current caused by step stimulus, while current recorded by the CCDAI does not contain the charging current. Due to unavoidable convection in the solution [31], the currents at the steady state fluctuate slightly in amplitude. This phenomenon was observed from the data

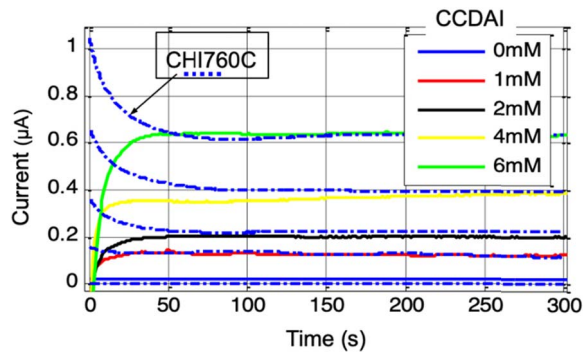


Fig. 15. Faradaic current recorded by the CCDAI at $V_{WE-RE} = 190$ mV as a function of time for 0–6 mM of potassium ferricyanide. The dot and dash curves present the data recorded by CHI760C for reference.

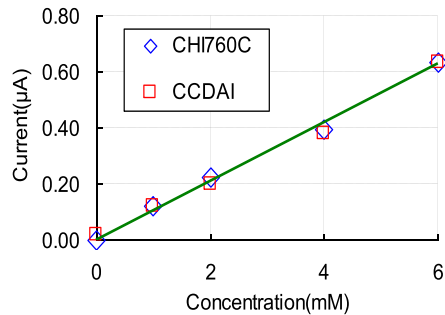


Fig. 16. Calibration curve of faradaic current versus potassium ferricyanide concentration. The current values were the average values from 200 to 300 s. Fitting curve was presented as a straight line. R^2 values of the fitting line are 0.991 and 0.996 for the data acquired by CCDAI and CHI760C, respectively.

recorded by both instrumentations. Results obtained from the CCDAI at different potassium ferricyanide concentrations are shown in Fig. 15. The data obtained from CHI760C are plotted as dot/dash curves as references. Steady-state current values recorded by the CCDAI and by CHI760C have good agreements with negligible differences in all tested concentration cases. The average current values from 200 to 300 s, which were recorded by CCDAI and CHI760C, were taken to plot the calibration curve as shown in Fig. 16. The least-squares correlation coefficients (R^2) of the fitting curve are 0.991 and 0.996 for the data acquired by CCDAI and CHI760C, respectively. The electrochemical experiment results demonstrate the functionality and accuracy of the CCDAI.

C. Analysis of Area and Power Savings

The CCDAI realizes a compact topology while maintaining the functionality of a traditional amperometric instrumentation circuit. Compared to the model instrumentation circuit shown in Fig. 2, the CCDAI (Fig. 8) eliminates two opamps and one integrator capacitor. In microelectronic circuits, both of these components usually occupy a larger area than comparators and current sources. In addition, opamps are a major source of power consumption in ICs. To provide a qualitative comparison, Tables I and II list the area and power consumption, respectively, of each component based on results from circuit blocks within a 0.5- μ m CMOS analog chip [32]. The total

TABLE I
AREA OCCUPATION OF IC BLOCKS IN A 0.5- μ m CMOS FABRICATION PROCESS FOR COMPARISON BETWEEN THE MODEL AMPEROMETRIC INSTRUMENTATION CIRCUIT AND THE CCDAI

	Area(μm^2)	Model	CCDAI	Savings
Opamp	1200	2	0	
Comparator	1000	1	1	
Current source pair (with switch)	600	1	1	
8-bit counter @100kHz	12000	1	1	
Capacitor(μF)	2200	1	0	
Total area(μm^2)		18200	13600	25%

TABLE II
POWER CONSUMPTION OF IC BLOCKS IN A 0.5- μ m CMOS FABRICATION PROCESS FOR THE COMPARISON BETWEEN THE MODEL AMPEROMETRIC INSTRUMENTATION CIRCUIT AND THE CCDAI

	Power@5V (μW)	Model	CCDAI	Savings
Opamp	7.5	2	0	
Comparator	5	1	1	
Current source pair (with switch)	0.5	1	1	
8-bit counter @100kHz	11	1	1	
Capacitor(1pF)	N/A	1	0	
Total power(μW)		31.5	16.5	47.6%

TABLE III
COMPARISON OF THE POTENTIostat WITH PREVIOUS WORK

Work	Tech	Supply	Resolution	Power (μW)	Area (mm^2)
[131] 2014	2.5 μm CMOS	5V	$\sim\mu\text{A}$	25	6.44
[141] 2016	0.18 μm CMOS	1.8V	50-200nA	71.7	0.0179
[151] 2012	0.13 μm CMOS	1.2V	150nA	3	0.36
[61] 2018	PCB	5v	$\sim\mu\text{A}$	12.6/CCM* 139/DCM*	
CCDAI	0.5 μm CMOS	5V		16.5 $^\Delta$	0.0136 $^\Delta$
	PCB	5V	6 nA	25	

* CCM: Continuous current mode; DCM: Discrete current mode;

$^\Delta$ Analytical calculation

estimated area and power of the potential CCDAI chip and the model electrochemical circuit are shown in the last row of the tables. The CCDAI reduces the area by 25.3% and power consumption by 47.6% compared to the model amperometric instrumentation circuit. Area savings can be further improved using an advanced process node; the large area digital counter would be much smaller and the area savings due to CCDAI's eliminating the integration capacitor would be amplified because capacitors do not scale with feature size. For further comparison, Table III shows the performance characteristics of several amperometric instrumentation circuits that also target low power applications. In comparison, our CCDAI design demonstrates good resolution and power performance while potentially utilizing a very low area.

VI. CONCLUSION

A novel compact amperometric instrumentation design with a current-to-digital readout for the electrochemical sensor was presented. Compared to a model amperometric instrumentation structure, the new design dramatically saves area, cost, and power by utilizing the sensor's double layer capacitor as a circuit element and adopting EIS mode, without sacrificing its resolution and detection of limitation performance. A board-level CCDAI was implemented and tested, demonstrating an 8-bit effective resolution in the range of -800 to 800 nA. The functionality of the instrumentation was verified by an electrochemical experiment in potassium ferricyanide. High linearity of current-to-concentration transfer was acquired with an R^2 of 0.991. A CMOS implementation of the CCDAI is estimated to save 25.3% of the area and 47.6% of power compared to the model amperometric instrumentation structure. Thus, this new compact circuit topology is well-suited for portable/wireless electrochemical sensor applications.

REFERENCES

- [1] J. R. Stetter, G. Korotcenkov, X. Zeng, Y. Tang, and Y. Liu, "Electrochemical gas sensors: Fundamentals, fabrication and parameters," *Chem. Sensors Comprehensive Sensor Technol.*, vol. 5, pp. 1–89, Jun. 2011.
- [2] J. Wang, "Electrochemical biosensors: Towards point-of-care cancer diagnostics," *Biosens. Bioelectron.*, vol. 21, no. 10, pp. 1887–1892, Apr. 2006.
- [3] S.-L. D. Kruppa Philipp *et al.*, "A digital CMOS-based 24×16 sensor array platform for fully automatic electrochemical DNA detection," *Biosensors Bioelectron.*, vol. 26, no. 4, pp. 1414–1419, Dec. 2010.
- [4] E. M. I. M. Ekanayake, D. M. G. Preethichandra, and K. Kaneto, "An amperometric glucose biosensor with enhanced measurement stability and sensitivity using an artificially porous conducting polymer," *IEEE Trans. Instrum. Meas.*, vol. 57, no. 8, pp. 1621–1626, Aug. 2008.
- [5] J. Park, C.-S. Kim, and M. Choi, "Oxidase-coupled amperometric glucose and lactate sensors with integrated electrochemical actuation system," *IEEE Trans. Instrum. Meas.*, vol. 55, no. 4, pp. 1348–1355, Aug. 2006.
- [6] S. Ghanbari, M. Habibi, and S. Magierowski, "A high-efficiency discrete current mode output stage potentiostat instrumentation for self-powered electrochemical devices," *IEEE Trans. Instrum. Meas.*, vol. 67, no. 9, pp. 2247–2255, Sep. 2018.
- [7] Y. Huang and A. J. Mason, "A redox-enzyme-based electrochemical biosensor with a CMOS integrated bipotentiostat," in *Proc. IEEE Biomed. Circuits Syst. Conf.*, Nov. 2009, pp. 29–32.
- [8] S. Martin, F. H. Gebara, T. D. Strong, and R. B. Brown, "A low-voltage, chemical sensor interface for systems-on-chip: The fully-differential potentiostat," in *Proc. IEEE Int. Symp. Circuits Syst.*, vol. 4, May 2004, p. 892.
- [9] M. M. Ahmadi and G. A. Jullien, "Current-mirror-based potentiostats for three-electrode amperometric electrochemical sensors," *IEEE Trans. Circuits Syst. I, Reg. Papers*, vol. 56, no. 7, pp. 1339–1348, Jul. 2009.
- [10] S. Ayers, K. D. Gillis, M. Lindau, and B. A. Minch, "Design of a CMOS potentiostat circuit for electrochemical detector arrays," *IEEE Trans. Circuits Syst. I, Reg. Papers*, vol. 54, no. 4, pp. 736–744, Apr. 2007.
- [11] A. Gore, S. Chakrabarty, S. Pal, and E. Alocilja, "A multi-channel femtoampere-sensitivity conductometric array for biosensing applications," in *Proc. Int. Conf. IEEE Eng. Med. Biol. Soc.*, Aug. 2006, pp. 6489–6492.
- [12] Y. Aleeva *et al.*, "Amperometric biosensor and front-end electronics for remote glucose monitoring by crosslinked PEDOT-glucose oxidase," *IEEE Sensors J.*, vol. 18, no. 12, pp. 4869–4878, Jun. 2018.
- [13] S. Sutula, J. P. Cuxart, J. Gonzalo-Ruiz, F. X. Munoz-Pascual, L. Teres, and F. Serra-Graells, "A $25\text{-}\mu\text{W}$ All-MOS potentiostatic delta-sigma ADC for smart electrochemical sensors," *IEEE Trans. Circuits Syst. I, Reg. Papers*, vol. 61, no. 3, pp. 671–679, Mar. 2014.
- [14] K. A. Al Mamun, S. K. Islam, D. K. Hensley, and N. McFarlane, "A glucose biosensor using CMOS potentiostat and vertically aligned carbon nanofibers," *IEEE Trans. Biomed. Circuits Syst.*, vol. 10, no. 4, pp. 807–816, Aug. 2016.
- [15] Y.-T. Liao, H. Yao, A. Lingley, B. Parviz, and B. P. Otis, "A $3\text{-}\mu\text{W}$ CMOS glucose sensor for wireless contact-lens tear glucose monitoring," *IEEE J. Solid-State Circuits*, vol. 47, no. 1, pp. 335–344, Jan. 2012.
- [16] H. Li, C. S. Boling, and A. J. Mason, "CMOS amperometric ADC with high sensitivity, dynamic range and power efficiency for air quality monitoring," *IEEE Trans. Biomed. Circuits Syst.*, vol. 10, no. 4, pp. 817–827, Aug. 2016.
- [17] H. Li, S. Parsnejad, E. Ashoori, C. Thompson, E. K. Purcell, and A. J. Mason, "Ultracompact microwatt CMOS current readout with picoampere noise and kilohertz bandwidth for biosensor arrays," *IEEE Trans. Biomed. Circuits Syst.*, vol. 12, no. 1, pp. 35–46, Feb. 2018.
- [18] S. S. Ghoreishzadeh, I. Taurino, G. De Micheli, S. Carrara, and P. Georgiou, "A differential electrochemical readout ASIC with heterogeneous integration of bio-nano sensors for amperometric sensing," *IEEE Trans. Biomed. Circuits Syst.*, vol. 11, no. 5, pp. 1148–1159, Oct. 2017.
- [19] M. H. Nazari, H. Mazhab-Jafari, L. Leng, A. Guenther, and R. Genov, "CMOS neurotransmitter microarray: 96-channel integrated potentiostat with on-die microsensors," *IEEE Trans. Biomed. Circuits Syst.*, vol. 7, no. 3, pp. 338–348, Jun. 2013.
- [20] M. Stanacevic, K. Murari, A. Rege, G. Cauwenberghs, and N. V. Thakor, "VLSI potentiostat array with oversampling gain modulation for wide-range neurotransmitter sensing," *IEEE Trans. Biomed. Circuits Syst.*, vol. 1, no. 1, pp. 63–72, Mar. 2007.
- [21] H. Li, X. Liu, L. Li, X. Mu, R. Genov, and A. J. Mason, "CMOS electrochemical instrumentation for biosensor microsystems: A review," *Sensors*, vol. 17, no. 1, p. 74, 2017.
- [22] X. Mu, *Wearable Gas Sensor Microsystem for Personal Healthcare and Environmental Monitoring*. 2013.
- [23] A. J. Bard and L. R. Faulkner, *Electrochemical Methods: Fundamentals and Applications*, vol. 8. 2000.
- [24] C. M. Pettit, P. C. Goonetilleke, C. M. Sulyma, and D. Roy, "Combining impedance spectroscopy with cyclic voltammetry: Measurement and analysis of kinetic parameters for faradaic and nonfaradaic reactions on thin-film gold," *Anal. Chem.*, vol. 78, no. 11, pp. 3723–3729, Apr. 2006.
- [25] S. M. Martin, F. H. Gebara, B. J. Larivee, and R. B. Brown, "A CMOS-integrated microinstrument for trace detection of heavy metals," *IEEE J. Solid-State Circuits*, vol. 40, no. 12, pp. 2777–2786, Dec. 2005.
- [26] P. M. Levine, P. Gong, R. Levicky, and K. L. Shepard, "Active CMOS sensor array for electrochemical biomolecular detection," *IEEE J. Solid-State Circuits*, vol. 43, no. 8, pp. 1859–1871, Aug. 2008.
- [27] L. Li, X. Liu, W. A. Qureshi, and A. J. Mason, "CMOS amperometric instrumentation and packaging for biosensor array applications," *IEEE Trans. Biomed. Circuits Syst.*, vol. 5, no. 5, pp. 439–448, Oct. 2011.
- [28] D. Kościelnik and M. Miśkiewicz, "Asynchronous sigma-delta analog-to-digital converter based on the charge pump integrator," *Analog Integr. Circuits Signal Process.*, vol. 55, no. 3, pp. 223–238, Jun. 2008.
- [29] M. E. Orazem and B. Tribollet, *Electrochemical Impedance Spectroscopy*. Hoboken, NJ, USA: Wiley, 2008.
- [30] *Analog Devices Document*, Analog Devices, Norwood, MA, USA, 2013.
- [31] J. A. Plambeck, *Electroanalytical Chemistry: Basic Principles and Applications*. New York, NY, USA: Wiley, 1982.
- [32] C. Yang, S. R. Jadhav, R. M. Worden, and A. J. Mason, "Compact low-power impedance-to-digital converter for sensor array microsystems," *IEEE J. Solid-State Circuits*, vol. 44, no. 10, pp. 2844–2855, Nov. 2009.



Heyu Yin received the B.S. degree in engineering management from Hubei University, Wuhan, China, and the master's degree in microelectronics and nanoelectronics from Tsinghua University, Beijing, China. He is currently pursuing the Ph.D. degree with the Department of Electrical and Computer Engineering, Michigan State University, East Lansing, MI, USA.

His current research interests include electrochemical sensor and lab-on-CMOS integration for portable biosensing and environmental monitoring application.



Ehsan Ashoori (S'–) received the B.S. and M.S. degrees in electrical engineering from K. N. Toosi University of Technology, Tehran, Iran, in 2009 and 2012, respectively. He is currently pursuing the Ph.D. degree with the Department of Electrical and Computer Engineering, Michigan State University, East Lansing, MI, USA.

His current research interests include wireless power and data telemetry, integrated circuits, and embedded systems for biomedical and environmental monitoring applications.



Xiaoyi Mu (S'11–M'13) received the B.S. and M.S. degrees in materials science from Fudan University, Shanghai, China, in 2004 and 2007, respectively, and the M.S. and Ph.D. degrees in electrical engineering from Michigan State University, East Lansing, MI, USA, in 2010 and 2013, respectively.

From 2007 to 2008, he was a Circuit Design Engineer with Integrated Device Technology Inc., Shanghai. He is currently a System Engineer with Apple Inc., Cupertino, CA, USA. His current research interests include analog and mixed-signal

IC design, electrochemical sensor, and system development.



Andrew J. Mason (S'90–M'99–SM'06) received the B.S. degree in physics with highest distinction from Western Kentucky University, Bowling Green, KY, USA, in 1991, the B.S.E.E. degree (Hons.) from the Georgia Institute of Technology, Atlanta, GA, USA, in 1992, and the M.S. and Ph.D. degrees in electrical engineering from the University of Michigan, Ann Arbor, MI, USA, in 1994 and 2000, respectively.

From 1999 to 2001, he was an Assistant Professor at the University of Kentucky. In 2001, he joined the Department of Electrical and Computer Engineering, Michigan State University, East Lansing, MI, USA, where he is currently a Professor. His current research interests include mixed-signal circuits, microfabricated structures and machine learning algorithms for integrated microsystems in biomedical, environmental monitoring, sustainable lifestyle applications, the design of augmented human awareness systems including signal processing algorithms and hardware for brain-machine interface, wearable/implantable biochemical and neural sensors, and lab-on-CMOS integration of sensing, instrumentation, and microfluidics.

Dr. Mason was a recipient of the 2006 Michigan State University Teacher-Scholar Award and the 2010 Withrow Award for Teaching Excellence. He serves on the Sensory Systems and Biomedical Circuits and Systems Technical Committees of the IEEE Circuits and Systems Society. He is an Associate Editor for the IEEE TRANSACTIONS ON BIOMEDICAL CIRCUITS AND SYSTEMS and serves on the Editorial Board for the *BioNanoScience Journal*. He serves on the technical and review committees for several IEEE conferences and was a Co-General Chair of the 2011 IEEE Biomedical Circuits and Systems Conference.